A Symmetric ADMM for Non-convex Regularization Magnetic Resonance Imaging

Zhijun Luo, Zhibin Zhu, and Benxin Zhang

***Abstract*—The total variation (TV) regularization technique is a popular method for magnetic resonance imaging (MRI) reconstruction. In this paper, the generalized minimax concave (GMC) penalty function is used to construct a nonconvex regularized MRI model, which can effectively prevent the systematic underestimation characteristic of the standard TV regularization. In addition, the cost function can maintain convexity under certain conditions. To solve the new non-convex model, we describe a symmetric alternating direction method of multipliers (S-ADMM) algorithm, which is faster than the original ADMM. The experiment results show the effectiveness of the proposed model and algorithm.**

***Index Terms*—MRI reconstruction, ADMM, TV regularization, minimax-concave penalty.**

1. Introduction

THE properties of non-radiation and non-ionizing make magnetic resonance imaging (MRI) have attracted considerable attention in the fields of medical. However, several constraints, such as nuclear relaxation times, signal to noise, power absorption, and so on, make MRI be a time consume procedure. Moreover, the longer the MRI, the more uncomfortable the patient will be, and the higher the possibility of artifacts will increase. Therefore, to cut back the acquisition time of MRI, a lot of techniques [1]-[6] have been developed. Among them, compressed sensing technology is particularly prominent and outstanding [5]-[6], since it is more likely to reconstruct the exact signal than the traditional Shannon-Nyquist sampling criterion demands when the signal is sparse, and some assumptions are met. Compressed sensing has become the focus of the MRI community since the invention of the pioneering work compression sensing MRI [7]-[8].

In MRI field, researchers commonly formulate the data acquisition as

$$\mathbf{y} = \underbrace{\mathbf{RF}}_{\mathbf{A}}\mathbf{x} + \varepsilon = \mathbf{Ax} + \varepsilon \tag{1.1}$$

where $\mathbf{x}$ and ε are the desired MR image and noise/disturbance, respectively; $\mathbf{R}$ and $\mathbf{F}$ denote the undersampling operator and the Fourier operator, respectively; $\mathbf{y}$ represents the undersampled k-space measurement, and its scale is much smaller than that of $\mathbf{x}$. MR image reconstruction aims to revover $\mathbf{x}$ from $\mathbf{y}$. Compressed sensing based reconstruction techniques commonly model the reconstruction as

$$\min_{\mathbf{x}} \lambda\|\mathbf{x}\|_{\mathrm{TV}} + \frac{1}{2}\|\mathbf{y} - \mathbf{Ax}\|_2^2, \tag{1.2}$$

where $\|\mathbf{x}\|_{\mathrm{TV}} = \|\mathbf{Dx}\|_1$ ($\mathbf{D}$ is finite difference operator), $\lambda > 0$ is the regularization parameter. If the matrix A satisfies some certain conditions, the classical TV regularization is described as a convex optimization problem with ℓ_1-norm regularization [6]. The minimizer of cost function is unique. However, the use of ℓ_1-norm regularization suffers from two limitations [9]-[10]: 1) the estimation for large coefficients may be biased, 2) it is unable to recover a signal by the least measurements. Therefore, many non-convex regularizations have been developed for dealing with these issues [11]-[20]. For instance, the ℓ_p-norm regularization was studied in [11]-[15], and its significantly better recovery performance than ℓ_1-regularization was verified. A kernel norm model [16] and ℓ_1-ℓ_2 model [17] is considered to deal with color image restoration, respectively. Inspired by the Moreau envelope and minimax-concave penalty, a nonseparable non-convex TV regularization was proposed in [18] and extended in [19]-[20]. Unfortunately, these non-convex regularizations cannot be directly applied to MRI models [22]. Based on the generalization of the minimax-concave (GMC) penalty, this paper proposes a non-convex regularization, particularly for MRI model. Under mild assumptions, the proposed non-convex regularization can keep convexity, and make the loss function be convex. Therefore, the corresponding MRI model can be solved by some popular convex optimization algorithms, which is another focus of researchers for MR image reconstruction [23]-[39]. Many fast algorithms have been developed using the structure and regularizers of the system model in MRI, such as augmented lagrangian methods (ALM) [23]-[24], primal-dual methods [25]-[26], splitting methods [27]-[29], the fast iterative soft thresholding algorithm (FISTA) [30]-[32], regularized Hermitian & skew-Hermitian splitting (RHSS) [33], alternating direction method of multipliers (ADMM) algorithm [34]-[38] etc. For more detailed discussion, please see [39]. In this paper, we will solve the proposed model by ADMM, which is simple in structure similar to the ALM and equivalent to some other splitting algorithms under certain conditions.

Manuscript received August 20, 2020; revised May 7, 2021. This work was supported in part by the National Natural Science Foundation of China under Grants 11901137, 61967004, in part by the Natural Science Foundation of Guangxi province under Grant 2018GXNSFBA281023, and in part by Scientific Research Fund of Hunan Provincial Education Department 20A273, in part by Research Fund of Mathematics Discipline of Hunan University of Humanities, Science and Technology 2020SXJJ01.

Zhijun, Luo is a PHD candidate in theSchool of Electronic Engineering and Automation, Guangxi Key Laboratory of Automatic Detecting Technology and Instruments, Guilin University of Electronic Technology, Guilin, 541004, P. R. China, and an associate Professor in the School of Mathematics and Finance, Hunan University of Humanities, Science and Technology, Loudi, 417000, P. R. China e-mail: ldlzj123@163.com.

Zhibin, Zhu is a Professor in the School of Mathematics and Computing Science, Guangxi Colleges and Universities Key Laboratory of Data Analysis and Computation, Guilin University of Electronic Technology, Guilin, 541004, P. R. China. Corresponding author, e-mail: optimization_zhu@163.com.

Benxin, Zhang is an associate Professor in the School of Electronic Engineering, Automation and Guangxi Key Laboratory of Automatic Detecting Technology and Instruments, Guilin University of Electronic Technology, Guilin, 541004, P. R. China. e-mail: bxzhang@guet.edu.cn.

The main contribution of this article can be summarized as following: 1) We construct a more accurate MRI reconstruction non-convex model via generalized minimax-concave (GMC) penalty function. The most important feature of the new model follows "convex non-convex" property, that is, although the GMC penalty is non-convex, it's easy to show the penalty maintain the convexity of the objective function under certain conditions. 2) To solve the proposed model, we introduce symmetric ADMM method with large step sizes. By choosing some appropriate values of (r, s), the symmetric ADMM method is better than the original ADMM. 3) In order to evaluate the performance, a number of experiments are carried out with different sampling masks and MR datasets.

The rest of this paper is organized as follows. Section 2 introduces the non-convex MRI reconstruction model. In Section 3, a new symmetric ADMM algorithm is presented. Section 4 contains experimental results. At last, some conclusions are made in Section 5.

2. Non-convex MRI reconstruction model

In this section, we recalled the definition of minimax-concave (MC) function, and defined the generalized minimax-concave (GMC) function. Second, we defined GMCTV regularization using the GMC penalty. Finally, we proposed a non-convex regularization model for MRI reconstruction and showed its properties.

Definition 2.1. *[18] The MC function $\phi : \mathbb{R} \to \mathbb{R}$ is defined as*

$$\begin{cases} \phi(x) = |x| - s(x), \\ s(x) = \min\limits_{v\in\mathbb{R}} \left\{ |v| + \frac{1}{2}(x-v)^2 \right\}. \end{cases} \tag{2.3}$$

The function $s(x)$ is also called Huber function. The Fig.1(a) illustrates the function $\phi(x)$ corresponding to $s(x)$.

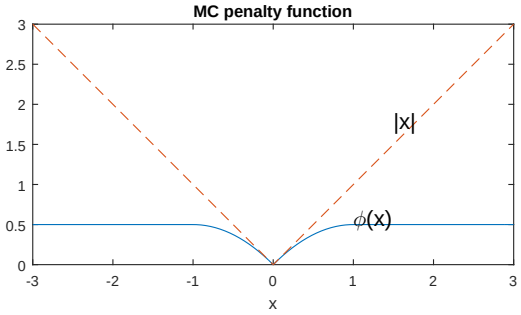

(a) MC penalty function.

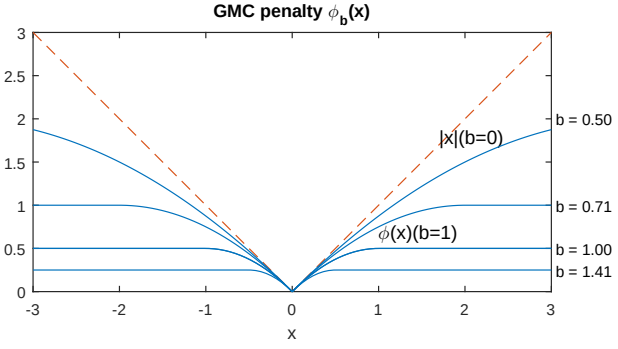

(b) GMC penalty function.

Fig. 1. MC and GMC penalty function

Definition 2.2. *For $\forall b \in \mathbb{R}$, the GMC penalty function $\phi_b : \mathbb{R} \to \mathbb{R}$ can be expressed as*

$$\begin{cases} \phi_b(x) = |x| - s_b(x), \\ s_b(x) = \min\limits_{v\in\mathbb{R}} \left\{ |v| + \frac{1}{2}b^2(x-v)^2 \right\}. \end{cases} \tag{2.4}$$

From the definition of the GMC penalty function and the description of Fig.1(b), naturally, we consider replacing x with gradient $\mathbf{Dx}$ in equation (2.4), which leads to our definition of GMCTV as follows.

Definition 2.3. *For $\forall b$, the GMC penalty function of non-convex TV regularizer: $\|\mathbf{x}\|_{GMCTV} : \mathbb{R}^{\mathbb{N}} \to \mathbb{R}$*

$$\begin{cases} \|\mathbf{x}\|_{GMCTV} = \Psi(\mathbf{x}) = \|\mathbf{Dx}\|_1 - s_b(\mathbf{x}), \\ s_b(\mathbf{x}) = \min\limits_{\mathbf{v}\in\mathbb{R}^{\mathbb{N}}} \left\{ \|\mathbf{v}\|_1 + \frac{b^2}{2}\|\mathbf{Dx}-\mathbf{v}\|_2^2 \right\}, \end{cases} \tag{2.5}$$

where $\mathbf{D}$ is the first-order difference matrix.

For the function $\mathbf{s_b(x)}$, it has the following properties.

Propsition 2.1. *Let $\alpha \geq 0$, the function $s_b(\mathbf{x})$ is convex, differentiable and satisfies*

$$0 \leqslant s_b(\mathbf{x}) \leqslant \|\mathbf{Dx}\|_1 \quad \forall \mathbf{x} \in \mathbb{R}^N. \tag{2.6}$$

Proof: 1) It's easy to see that the function $s_b(\mathbf{x})$ is convex from the definition. Furthermore, we can obtain the function $s_b(\mathbf{x})$ is differentiable in view of the issue [18].
2) Obviously, $s_b(\mathbf{x}) \geq 0$ is true. From (2.5), for all $\mathbf{v}$, we can obtain

$$s_b(\mathbf{x}) \leqslant \|\mathbf{v}\|_1 + (b^2/2)\|\mathbf{Dx}-\mathbf{v}\|_2^2.$$

Let $\mathbf{v} = \mathbf{Dx}$, it implies that $s_b(\mathbf{x}) \leqslant \|\mathbf{Dx}\|_1$, i.e., the inequality (2.6) holds. □

Then, we consider the following formulation for MRI

$$\min_{\mathbf{x}} \lambda\Psi(\mathbf{x}) + \frac{1}{2}\|\mathbf{y}-\mathbf{Ax}\|_2^2, \tag{2.7}$$

where $\Psi(\mathbf{x})$ is given by (2.5), $\lambda > 0$ is called regularization parameter. For $\Psi(\mathbf{x})$ is non-convex, the model (2.7) is non-convex model. If the parameter b is correctly limited, the model (2.7) has the following characteristics:

Theorem 2.1. *Let $\lambda > 0$, $\alpha > 0$, define $G_b(\mathbf{x})$ as*

$$G_b(\mathbf{x}) = \frac{1}{2}\|\mathbf{y}-\mathbf{Ax}\|_2^2 + \lambda\Psi(\mathbf{x}), \tag{2.8}$$

if $\mathbf{A^TA} - \lambda b^2\mathbf{D^TD} \succeq \mathbf{0}$, then $G_b(\mathbf{x})$ is convex.

Proof: The cost function can be expressed as

$$\begin{aligned}\mathbf{G_b}(\mathbf{x}) &= \frac{1}{2}\|\mathbf{y}-\mathbf{Ax}\|_2^2+\lambda\|\mathbf{Dx}\|_1-\lambda s_b(\mathbf{x})\\ &= \frac{1}{2}\|\mathbf{y}-\mathbf{Ax}\|_2^2+\lambda\|\mathbf{Dx}\|_1\\ &\quad-\lambda\min_{\mathbf{v}}\{\|\mathbf{v}\|_1+\frac{b^2}{2}\|\mathbf{Dx}-\mathbf{v}\|_2^2\}\\ &= \max_{\mathbf{v}}\{\frac{1}{2}\|\mathbf{y}-\mathbf{Ax}\|_2^2+\lambda\|\mathbf{Dx}\|_1\\ &\quad-\lambda\|\mathbf{v}\|_1-\frac{\lambda b^2}{2}\|\mathbf{Dx}-\mathbf{v}\|_2^2\}\\ &= \max_{\mathbf{v}}\{\frac{1}{2}\mathbf{x}^T(\mathbf{A^TA}-\lambda b^2\mathbf{D^TD})\mathbf{x}\\ &\quad+\lambda\|\mathbf{Dx}\|_1+\mathbf{g}(\mathbf{x},\mathbf{v})\}\\ &= \frac{1}{2}\mathbf{x}^T(\mathbf{A^TA}-\lambda b^2\mathbf{D^TD})\mathbf{x}\\ &\quad+\lambda\|\mathbf{Dx}\|_1+\max_{\mathbf{v}}\mathbf{g}(\mathbf{x},\mathbf{v}),\end{aligned}$$

where $\mathbf{g}(\mathbf{x},\mathbf{v})$ is affine of $\mathbf{x}$, which implies $\max_{\mathbf{v}}\mathbf{g}(\mathbf{x},\mathbf{v})$ is convex. Hence, if $\mathbf{A^TA}-\lambda b^2\mathbf{D^TD}\succeq\mathbf{0}$ holds, the cost function $\mathbf{G_b}(\mathbf{x})$ is a convex function. □

3. Proposed Algorithm

We rewrite the problem (2.7) as following:

$$\begin{cases}\min\limits_{\mathbf{x}}\lambda(\|\mathbf{Dx}\|_1-\min\limits_{\mathbf{v}}\{\|\mathbf{v}\|_1+\\ \quad\frac{\alpha}{2}\|\mathbf{Dx}-\mathbf{v}\|_2^2\})+\frac{1}{2}\|\mathbf{y}-\mathbf{Ax}\|_2^2,\end{cases}\tag{3.9}$$

where $\alpha=b^2\geq 0$. The problem (3.9) can be equivalently expressed as

$$\min_{\mathbf{x}}\lambda\Psi(\mathbf{z})+\frac{1}{2}\|\mathbf{y}-\mathbf{Ax}\|_2^2,\ \text{s.t}\ \mathbf{z}=\mathbf{Dx}.\tag{3.10}$$

Hence, the augmented Lagrangian function of (3.10) can be written as

$$\begin{cases}\mathcal{L}(\mathbf{x},\mathbf{z},\mathbf{w})=\lambda\Psi(\mathbf{z})+\frac{1}{2}\|\mathbf{y}-\mathbf{Ax}\|_2^2\\ \quad-\mathbf{w^T}(z-\mathbf{Dx})+\frac{\rho}{2}\|\mathbf{z}-\mathbf{Dx}\|_2^2,\end{cases}\tag{3.11}$$

where $\Psi(\mathbf{z})=\|\mathbf{z}\|_1-\min_{\mathbf{v}}\{\|\mathbf{v}\|_1+\frac{\alpha}{2}\|\mathbf{z}-\mathbf{v}\|_2^2\}$, $\mathbf{w}$ is a Lagrange multiplier and $\rho>0$ is a penalty parameter. According to the standard ADMM, the iterative scheme of the problem (3.10) can be expressed as solving the following sub-problems

$$\begin{cases}\mathbf{x}^{k+1} &= \operatorname{argmin}\mathcal{L}(\mathbf{x},\mathbf{z^k},\mathbf{w^k})\\ &= \operatorname{argmin}_{\mathbf{x}}\{\frac{1}{2}\|\mathbf{y}-\mathbf{Ax}\|_2^2+\mathbf{w}^{kT}\mathbf{Dx}\\ &\quad+\frac{\rho}{2}\|\mathbf{z^k}-\mathbf{Dx}\|_2^2\},\\ \mathbf{z}^{k+1} &= \operatorname{argmin}\mathcal{L}(\mathbf{x^{k+1}},\mathbf{z},\mathbf{w^k})\\ &= \operatorname{argmin}_{\mathbf{z}}\{\lambda\Psi(\mathbf{z})-\mathbf{w^{kT}z}\\ &\quad+\frac{\rho}{2}\|\mathbf{z}-\mathbf{Dx^{k+1}}\|_2^2\},\\ \mathbf{w}^{k+1} &= \mathbf{w}^k-\rho(\mathbf{Dx^{k+1}}-\mathbf{z}^{k+1}).\end{cases}\tag{3.12}$$

As analyzed in [40], the primal variables $\mathbf{x}$ and $\mathbf{z}$ should be treated fairly. Hence, we consider using symmetric ADMM (S-ADMM) to solve the problem (3.10). Since Lagrange multipliers are updated twice at each iteration, its performance is often better than that of the original ADMM method. The S-ADMM iterative scheme for (3.10) can be written as

$$\begin{cases}\mathbf{x}^{k+1} &= \operatorname{argmin}\mathcal{L}(\mathbf{x},\mathbf{z^k},\mathbf{w^k})\\ &= \operatorname{argmin}_{\mathbf{x}}\{\frac{1}{2}\|\mathbf{y}-\mathbf{Ax}\|_2^2+\mathbf{w}^{kT}\mathbf{Dx}\\ &\quad+\frac{\rho}{2}\|\mathbf{z^k}-\mathbf{Dx}\|_2^2\},\\ \mathbf{w}^{k+\frac{1}{2}} &= \mathbf{w}^k-s\rho(\mathbf{Dx^{k+1}}-\mathbf{z}^k),\\ \mathbf{z}^{k+1} &= \operatorname{argmin}\mathcal{L}(\mathbf{x^{k+1}},\mathbf{z},\mathbf{w^{k+\frac{1}{2}}})\\ &= \operatorname{argmin}_{\mathbf{z}}\{\lambda\Psi(\mathbf{z})-\mathbf{w^{(k+\frac{1}{2})T}z}\\ &\quad+\frac{\rho}{2}\|\mathbf{z}-\mathbf{Dx^{k+1}}\|_2^2\},\\ \mathbf{w}^{k+1} &= \mathbf{w}^{k+\frac{1}{2}}-r\rho(\mathbf{Dx^{k+1}}-\mathbf{z}^{k+1}),\end{cases}\tag{3.13}$$

where the feasible region of s,r is

$$(s,r)\in\mathcal{D}=\Big\{s\in(-1,1),r\in\Big(0,\frac{1+\sqrt{5}}{2}\Big)\\ \&\ r+s>0,|s|<1+r-r^2\Big\}.$$

Now, we show how to solve the subproblems in (3.13). For $\mathbf{x}$-minimization step, the optimization subproblem for $\mathbf{x}^{k+1}$ can be solved via the first-order optimality optimality conditions,

$$\mathbf{x}^{k+1}=(\rho\mathbf{D^TD}+\mathbf{A^TA})^{-1}\widehat{\mathbf{W^k}},\tag{3.14}$$

where $\widehat{\mathbf{W^k}}=(\rho\mathbf{D^Tz^k}+\mathbf{A^Ty}-\mathbf{D^Tw^k})$. In the field of MRI, $\mathbf{A}=\mathbf{RF}$ ($\mathbf{F}$ is the Fourier operator such that $\mathbf{F}=\mathbf{F^{-1}}$), and $\mathbf{D^TD}$ is circulate matrix which can diagonalize via Fourier transform. For simplicity, we can get the optimal solution of $\mathbf{x^{k+1}}$ through two Fourier transforms.

For $\mathbf{z}$-minimization sub-problem:

$$\begin{aligned}\mathbf{z}^{k+1} &= \min_{\mathbf{z}}\{\lambda\Psi(\mathbf{z})-\lambda\mathbf{w^{(k+\frac{1}{2})T}z}\\ &\quad+\frac{\lambda\rho}{2}\|\mathbf{z}-\mathbf{Dx^{k+1}}\|_2^2\}\\ &= \min_{\mathbf{z}}\{\Psi(\mathbf{z})\\ &\quad+\frac{\rho}{2}\|\mathbf{z}-(\mathbf{Dx^{k+1}}+\frac{\mathbf{w^{k+\frac{1}{2}}}}{\rho})\|_2^2\}\end{aligned}\tag{3.15}$$

Follows the reference [18], we can write the iteration procedure below

$$\begin{cases}t^k &= \mathbf{Dx^{k+1}}+\frac{\mathbf{w^{k+\frac{1}{2}}}}{\rho}\\ &\quad+\frac{\alpha}{\rho}\big(z^k-\mathrm{tvd}(z^k;1/\alpha)\big)\\ z^{k+1} &= \mathrm{tvd}(t^k;\frac{1}{\rho})\end{cases}\tag{3.16}$$

where α is nonconvexity parameter,

$$\mathrm{tvd}(y;\lambda)=\min_x\{\lambda\|x\|_1+\frac{1}{2}\|y-x\|_2^2\}.\tag{3.17}$$

As shown in theorem 2.1, the convexity of the objective function is controlled by the value of α. For problem (3.17), we can use iterative shrinkage threshold algorithm (ISTA) [30]-[31] to solve.

Now, we propose an iterative algorithm for solving the problem (3.10). Since the GMCTV regular term is used in the model (3.10) and the symmetry property is used in the algorithm, we call this algorithm the symmetrization-GMCTV method (S-GMCTV).

Algorithm (S-GMCTV):

Step 0: Initialization and date.

Input parameters $\alpha\geq 0,\rho>0,\lambda>0$, $(r,s)\in\mathcal{D}$, the tolerance $\varepsilon>0$. Given $(\mathbf{x},\mathbf{z},\mathbf{w}):=(\mathbf{x^0},\mathbf{z^0},\mathbf{w^0})$, let $k:=0$;

Step 1: Compute the new iterate by (3.18);

$$\begin{cases} \mathbf{x^{k+1}} &= (\mathbf{A^T A} + \rho \mathbf{D^T D})^{-1} \widehat{\mathbf{W^k}}, \\ \mathbf{w}^{k+\frac{1}{2}} &= \mathbf{w}^k - r\rho(\mathbf{D x^{k+1}} - \mathbf{z}^k), \\ \mathbf{z}^{k+1} &= \mathrm{tvd}(t^k; \frac{1}{\rho}), \\ \mathbf{w}^{k+1} &= \mathbf{w}^{k+\frac{1}{2}} - s\rho(\mathbf{D x^{k+1}} - \mathbf{z}^{k+1}), \end{cases} \tag{3.18}$$

where $\widehat{\mathbf{W^k}} = (\rho \mathbf{D^T z^k} + \mathbf{A^T y} - \mathbf{D^T w^k})$,
$t^k = \mathbf{D x^{k+1}} + \frac{\mathbf{w^{k+\frac{1}{2}}}}{\rho} + \frac{\alpha}{\rho}\big(z^k - \mathrm{tvd}(z^k; 1/\alpha)\big)$.
Let $\widetilde{\mathbf{w}}^{\mathbf{k+1}} = (\mathbf{x^{k+1}}, \mathbf{z^{k+1}}, \mathbf{w^{k+1}})$.

Step 2: If $\|\widetilde{\mathbf{w}}^{\mathbf{k}} - \widetilde{\mathbf{w}}^{\mathbf{k+1}}\|_{\mathbf{2}}^{\mathbf{2}} \leq \varepsilon$, STOP; otherwise let $k =: k+1$. Go back to step 1.

Note: If $s = 0$, $r = 1$, the S-ADMM is the classical ADMM algorithm. The performance of the algorithm can be improved by selecting an appropriate $(s, r) \in \mathcal{D}$ value.

4. Numerical results

In this section, we evaluate the performance of the proposed S-GMCTV method through some numerical experiments, and compare the proposed method with those of classic TV [34] and MCTV [22]. All of our test experiments are performed on MATLAB R2015a on the PC with Intel(R) Core(TM) 2.2 GHz CPU and and 8.0 GB RAM.

MRI test images recovery performance was evaluated by peak signal-to-noise ratio (PSNR) and relative error (RE), which are respectively defined as

$$\mathrm{PSNR} = 10\mathrm{lg}\left(\frac{\|\mathbf{x} - \overline{\mathbf{x}}\|_2^2}{\|\mathbf{x}^k - \mathbf{x}\|_2^2}\right), \mathrm{RE} = \frac{\|\mathbf{x}^k - \mathbf{x}\|_2^2}{\|\mathbf{x}\|_2^2}.$$

where $\mathbf{x}$ is the original image, $\overline{\mathbf{x}}$ denotes the mean intensity value of $\mathbf{x}$, $\mathbf{x}^k$ is the restored image.

The sampling templates and the test MR images are shown in Fig. 2: (a) is the radial sampling with 10 trajectory lines. (b) is the pseudo-radial mask with 84 readout lines. (c) is Cartesian under-sampling mask with a sampling rate of 34%. (d)-(f) are test images (sizes 256×256): Shepp Logan, Brain angiography, Brain respectively. More details can be found in [22], [41]. We set the parameters as: $\lambda = 0.01$, $\delta_1 = \delta_2 = 0.0001$, $\rho = 150$, $(s, r) = (0.382, 1.618)$. In order to ensure that the objective function in the MCTV (or GMCTV) model is convex, let $\alpha = 0.05/\lambda$. To achieve higher PSNR, (s, r) could be set within the range of $\mathcal{D}$.

The numerical experiments are divided into four parts. In the first part of the numerical experiment, we showed the reconstruction effects of different MRI test images and three sampling templates under different models. From Figs 3-5, we can see the visual comparison of MRI reconstruction results under the different models. In Fig. 3, Shepp Logan phantom is chosen to evaluate the performance of the proposed S-GMCTV method. We compare with the three reconstruction models (TV, MCTV, S-GMCTV) proposed above under the radial sampling template. From the results, we can see that our S-GMCTV method reconstructed Shepp Logan image with $PSNR = 29.48$, which higher TV, MCTV methods. That is to say, The performance of S-GMCTV is better than that of TV and MCTV. Because the Cartesian undersampling is k-space data, and is most widely used in practice. For MR image Brain, we test the image by using the Cartesian template mask under 0.34 sampling rate. The

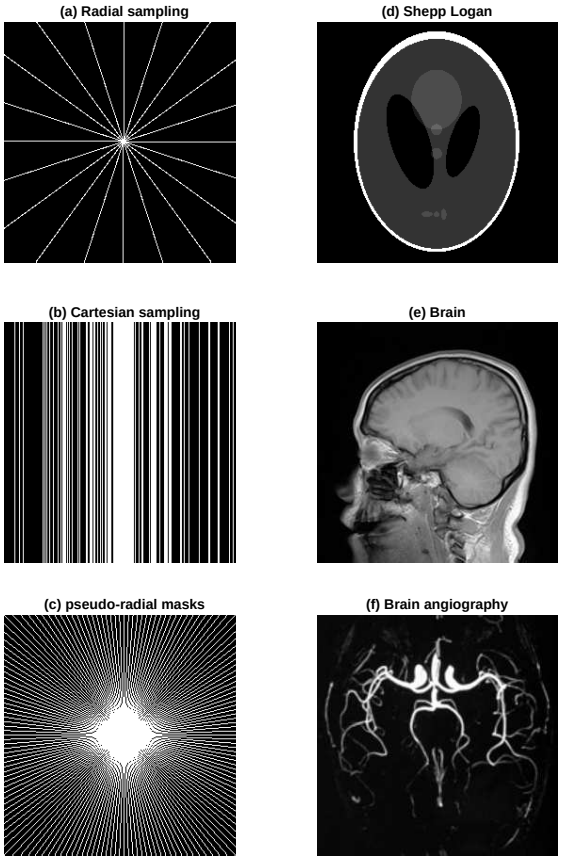

Fig. 2. Experimental datasets

reconstruction results were shown in Fig. 4. Then, we test S-GMCTV method on Brain angiography image under pseudo-radial masks with 84 readout lines. The reconstruction and error images were shown in Fig. 5. Through the visual comparison and analysis of the reconstruction results of three different methods shown in Figs. 3-5, it can conclude that the S-GMCTV always obtains better reconstruction results than the other two reconstruction models.

Table I reports the PSNR and RE of Brain Brain (256×256) and Brain angiography Brain (256×256) under a radial sampling template with 10 lines, pseudo-radial masks with 84 readout lines and Cartesian undersampling mask of sampling rate 34%. Compared with TV and MCTV, S-GMCTV method is more trustworthy and has better performance in testing MR images recovery, because it attained the higher PSNR and lower RE.

In the second part, we chose the Brain angiography image and radial sampling mask to evaluate the performance of the sampling rates. In the Fig. 6, the curves illustrate comparison of assessment indices PSNR and RE versus sampling rate under the different methods. Fig. 6(a) shows the RE curve versus the sampling rate. The curve shows that the value of RE decreases with the increase of sampling rate. And it can be observed that the RE value of S-GMCTV is lower than that of TV and MCTV under the same sampling rate. Fig. 6(b) gives the PSNR curve versus the sampling rate. The curve indicates that the value of PSNR increase with the increase of sampling rate. And it can be observed that the PSNR value of S-GMCTV is higher than that of TV and MCTV under the same sampling rate.

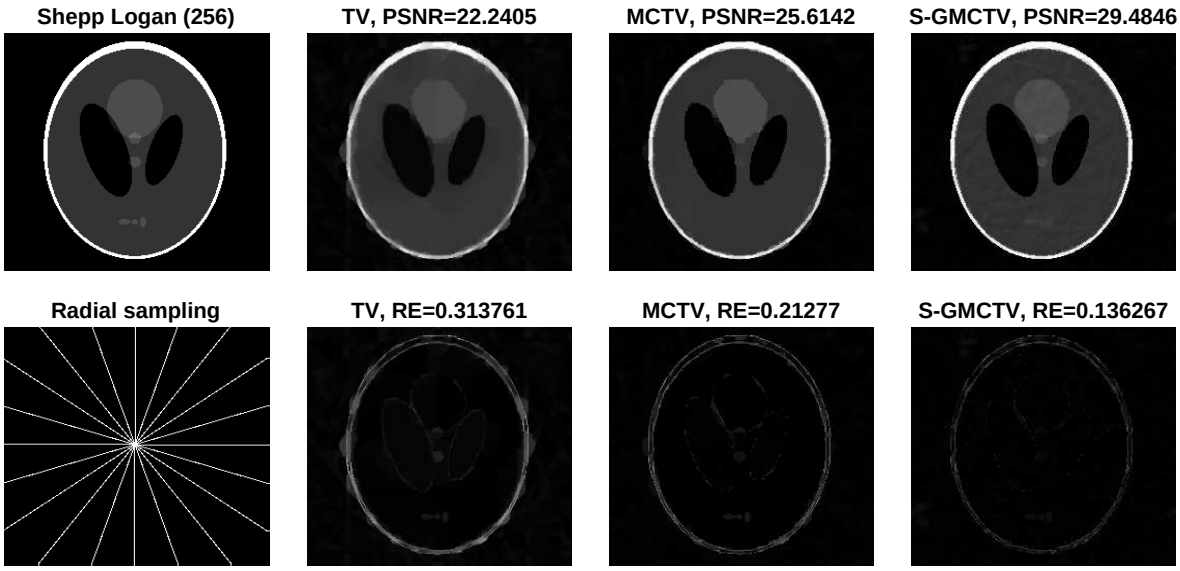

Fig. 3. Different reconstruction results of Shepp Logan (256×256) under Radial sampling

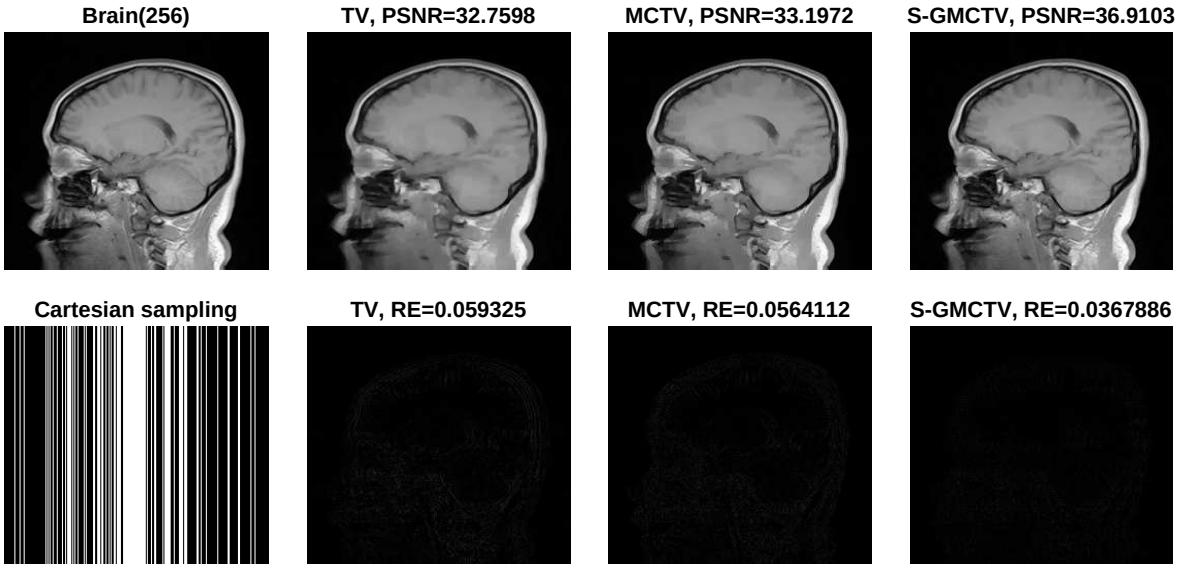

Fig. 4. Different reconstruction results of Brain (256×256) under Cartesian sampling

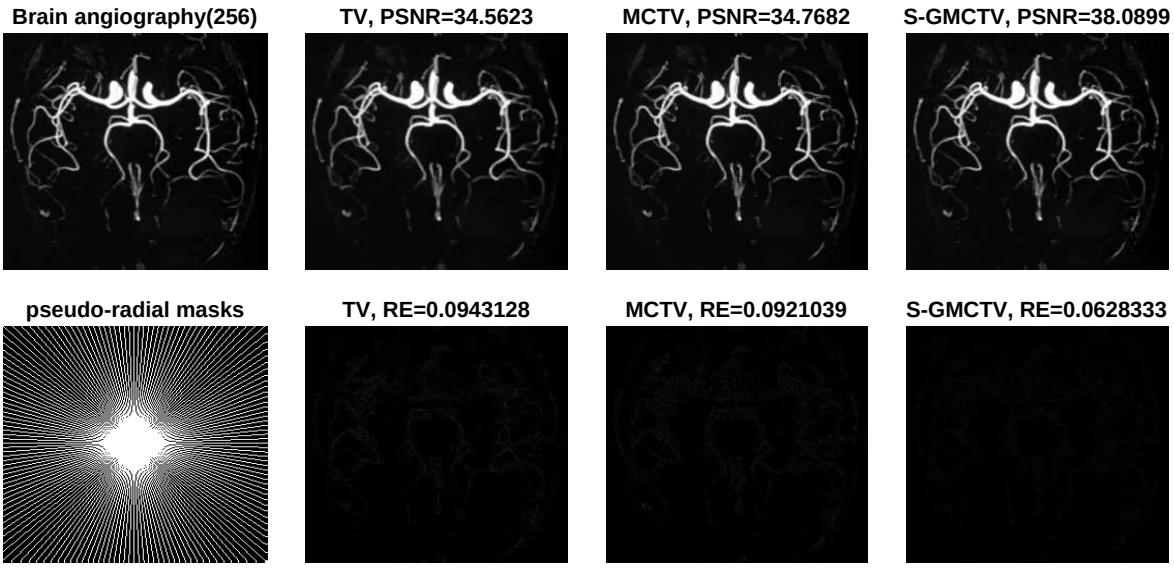

Fig. 5. Different reconstruction results of Brain angiography (256×256) under pseudo-radial masks

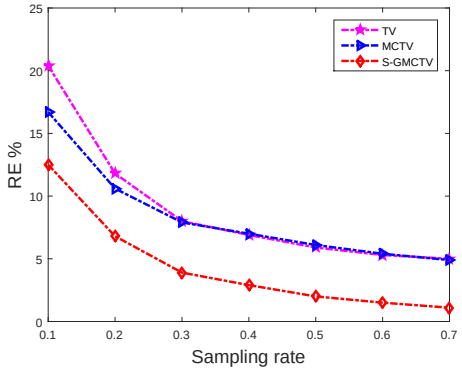

(a) Sampling rate VS RE

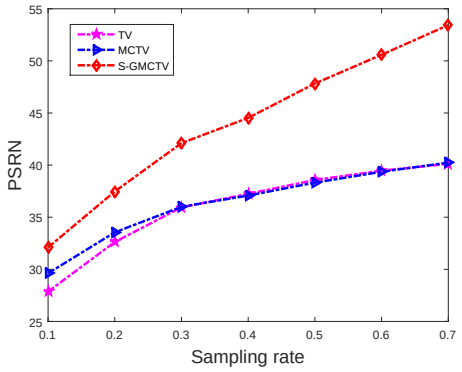

(b) Sampling rate VS PSNR

Fig. 6. PSNR and RE versus sampling rate on Brain angiography with three reconstruction models under the radial sampling template

In the third part of the numerical experiment, we select some representative values from $(s,r) \in \mathcal{D}$ such that the symmetric-ADMM is slightly faster than the original ADMM (i.e. $(s,r) = (0,1)$). For $r \in \left(0, \frac{1+\sqrt{5}}{2}\right)$, we mainly consider $r \approx 1.618$ (the golden ratio). The numerical experimental results from Table II show that the point $(s,r) = (0, 382, 1.618)$ is better some other points such as $(s,r) = (0, 1.618)$ and $(s,r) = (-0, 382, 1.618)$. Hence, for the sake of brevity, we have omitted the comparison with other points.

At the end of the experiment, we choose two 512×512 test images to illustrate the effectiveness of the proposed method. In Fig. 7, the Shepp Logan data (512) were measured using a radial sampling template with 15 lines under 3% sampling rate. It is obvious that S-GMCTV achieves about 3.6dB and 7.1dB performance gain as compared with MCTV and TV, respectively. For Brain (512), random sampling template with 10% sampling rate and 0.05 sampling radius was employed. Fig. 8 shows clearly that the reconstruction result of S-GMCTV method is superior than MCTV and TV methods.

5. Conclusion

In this paper, the GMCTV non-convex regularization term is constructed by using minimax-concave (GMC) penalty function, and we apply it to MR image reconstruction. Compared with classical TV regularizer, the GMCTV regularization term not only preserves the convexity of the objective function but also avoids the suboptimal local solutions. In order to accelerate the imaging speed, we introduce symmetric ADMM method with large step sizes. Numerical experiments show that the S-GMCTV method proposed in this paper can significantly improve the MRI reconstruction effect. In the future, this proposed method should be tested for more sparse systems such as dynamic magnetic resonance imaging etc.

Acknowledgment

The authors would like to thank Prof. Ivan Selesnick (http://eeweb.poly.edu/iselesni/index.html), Prof. Xiaobo Qu (https://csrc.xmu.edu.cn/index_cn/xiaobo/index_cn.html), and Dr. Yilin Liu (https://github.com/MrCredulous/MCTV-Image-Reconstruction) for sharing their Data, MATLAB code and free download from their homepages.

TABLE I
THE VALUE OF PSN AND RE UNDER DIFFERENT SAMPLING TEMPLATES.

Test Image	Template	Method	RE	PSNR
Brain	Radial sampling	TV	0.2011	22.1566
		MCTV	0.1874	22.7697
		S-GMCTV	**0.1793**	**23.1534**
	Cartesian sampling	TV	0.0593	32.7598
		MCTV	0.0564	33.1972
		S-GMCTV	**0.0368**	**36.9103**
	pseudo-radial masks	TV	0.0550	33.4165
		MCTV	0.0580	32.961
		S-GMCTV	**0.0426**	**35.6429**
Brain angiography	Radial sampling	TV	0.4045	21.9149
		MCTV	0.3628	22.8605
		S-GMCTV	**0.3384**	**23.4650**
	Cartesian sampling	TV	0.1169	32.6999
		MCTV	0.0955	34.4580
		S-GMCTV	**0.0629**	**38.0761**
	pseudo-radial masks	TV	0.0943	34.5623
		MCTV	0.0921	34.7682
		S-GMCTV	**0.0628**	**38.0899**

TABLE II
RECONSTRUCTION RESULTS UNDER DIFFERENT VALUES OF (r, s)

Test Image	Template	S-GMCTV	RE	PSNR
Shepp Logan	Radial sampling	$s = 0.000, r = 1.000$	0.1691	27.6088
		$s = 0.000, r = 1.618$	0.1689	27.6190
		$s = -0.382, r = 1.618$	0.2043	25.9681
		$\mathbf{s = 0.382, r = 1.618}$	**0.1363**	**29.4846**
Brain	Cartesian sampling	$s = 0.000, r = 1.000$	0.0385	36.5201
		$s = 0.000, r = 1.618$	0.0384	36.5410
		$s = -0.382, r = 1.618$	0.0372	36.8152
		$\mathbf{s = 0.382, r = 1.618}$	**0.0368**	**36.9103**
Brain angiography	pseudo-radial masks	$s = 0.000, r = 1.000$	0.0672	37.5034
		$s = 0.000, r = 1.618$	0.0667	37.5655
		$s = -0.382, r = 1.618$	0.0643	37.8932
		$\mathbf{s = 0.382, r = 1.618}$	**0.0628**	**38.0899**

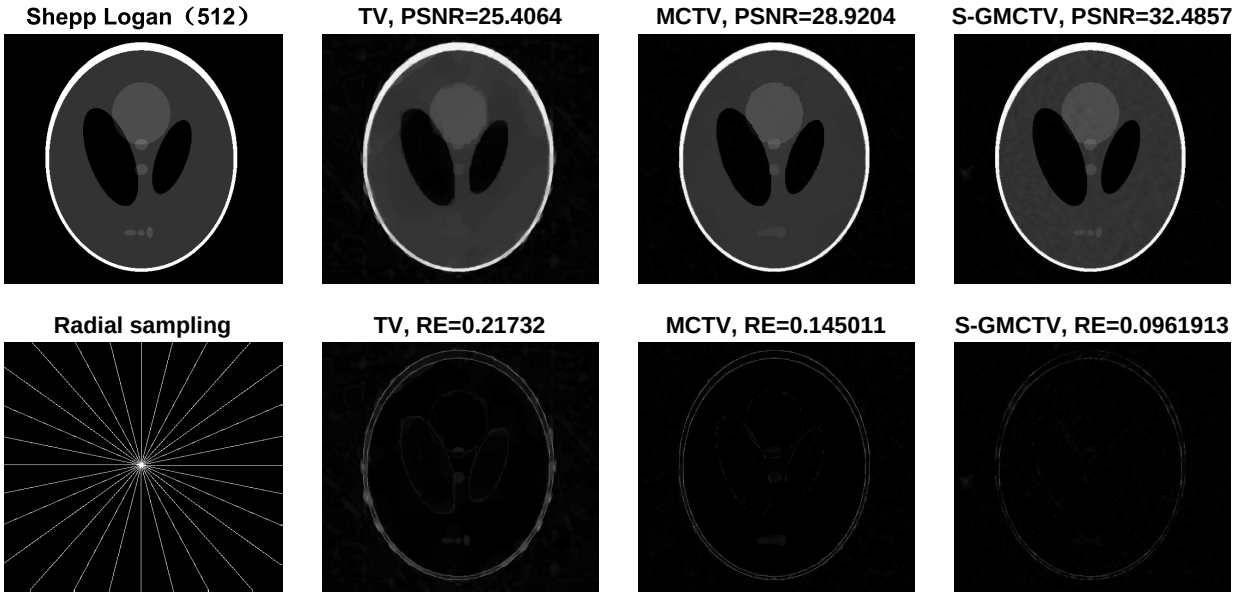

Fig. 7. Different reconstruction results of Shepp Logan (512×512) under Radial sampling

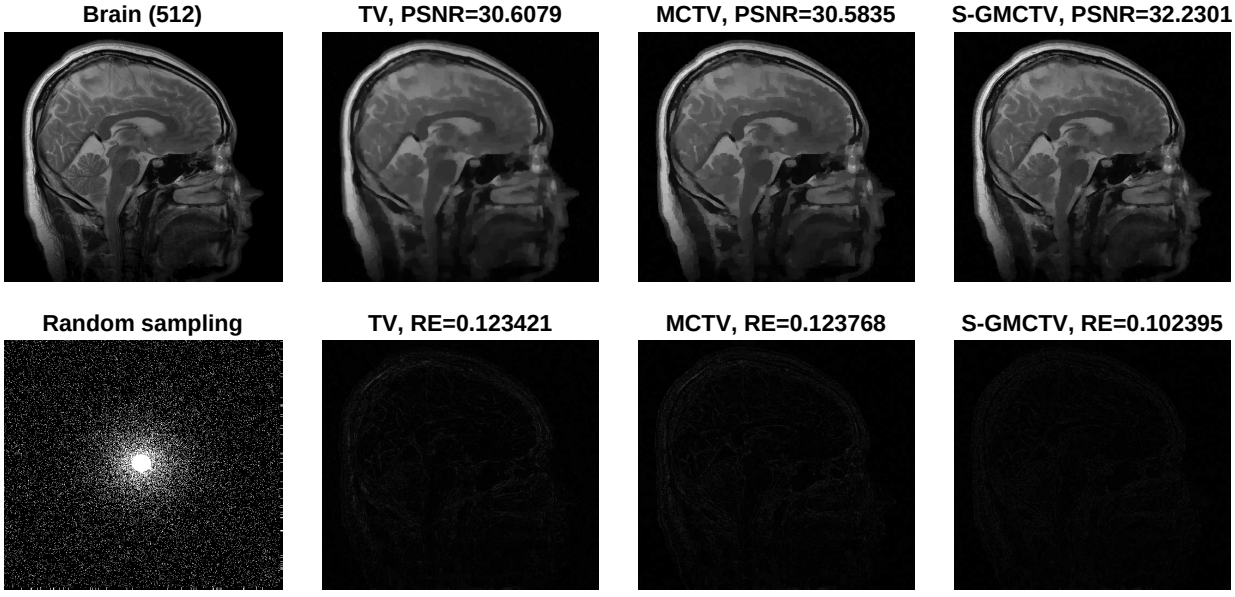

Fig. 8. Different reconstruction results of Brain (512×512) under Random sampling

REFERENCES

[1] P. Mansfield, "Multi-planar image formation using NMR spin echoes," *Journal of Physics C: Solid State Physics*, vol. 10, no. 3, pp. 55-58, 1977.

[2] A. Haase, J. Frahm, D. Matthaei, et al, "FLASH imaging rapid NMR imaging using low flip-angle pulses," *Journal of Magnetic Resonance*, vol. 67, no. 2, pp. 258-266, 1986.

[3] M. Hutchinson, U. Raff, "Fast MRI data acquisition using multiple detectors," *Magnetic Resonance in Medicine*, vol. 6, no. 1, pp. 87-91, 1988.

[4] D. Larkman, R. Nunes, "Parallel magnetic resonance imaging," *Phys. Med. Biol.*, vol. 52, no. 7, pp. 15-55, 2007.

[5] D. Donoho, "Compressed sensing," *IEEE Transactions on Information Theory*, vol. 52, no. 4, pp. 1289-1306, 2006.

[6] E. Candes, J. Romberg, T. Tao, "Robust uncertainty principles: exact signal reconstruction from highly incomplete frequency information," *IEEE Transactions on Information Theory*, vol. 52, no. 2, pp. 489-509, 2006.

[7] M. Lustig, D. Donoho, J. M. Pauly, "Sparse MRI: The application of compressed sensing for rapid MR imaging," *Magnetic Resonance in Medicine*, vol. 58, no. 6, pp. 1182-1195, 2007.

[8] M. Lustig, D. Donoho, J. Santos, et al, "Compressed Sensing MRI," *IEEE Signal Processing Magazine*, vol. 25, no. 2, pp. 72-82, 2008.

[9] R. Chartrand, V. Staneva, "Restricted isometry properties and non-convex compressive sensing," *Inverse Problems*, vol. 24, no. 3, pp. 035020, 2008.

[10] E. Candes, M. Wakin, S. Boyd, "Enhancing sparsity by reweighted ℓ_1 minimization," *Journal of Fourier Analysis and Applications*, vol. 14, pp. 877-905, 2008.

[11] S. Foucart, M. Lai, "Sparsest solutions of underdetermined linear systems via ℓ_q-minimization for $0 < q \leq 1$," *Applied and Computational Harmonic Analysis*, vol. 26, no. 3, pp. 395-407, 2009.

[12] I. Daubechies, R. Devore, M. Fornasier, et al, "Iteratively reweighted least squares minimization for sparse recovery," *Communications on Pure and Applied Mathematics*, vol. 63, no. 1, pp. 1-38, 2010.

[13] M. Lai, Y. Xu and W. Yin, "Improved iteratively reweighted least squares for unconstrained smoothed ℓ_q minimization," *SIAM Journal on Numerical Analysis*, vol. 51, no. 2, pp. 927-957, 2013.

[14] J. Pant, W. Lu, A. Antoniou, et al, "New improved algorithms for compressive sensing based on ℓ_p norm," *IEEE Transactions on Circuits and Systems Ii-express Briefs*, vol. 61, no. 3, pp. 198-202, 2014.

[15] F. Wen, L. Chu, P. Liu, et al, "A Survey on nonconvex regularization-based sparse and low-rank recovery in signal processing, statistics, and machine learning," *IEEE Access*, vol. 6, no.12, pp. 69883-69906, 2018.

[16] X. Guo, F. Liu, Y. Chen, et al, "Warm start of multi-channel weighted nuclear norm minimization for color image denoising," *IAENG International Journal of Computer Science*, vol. 46, no. 4, pp. 575-581, 2019.

[17] X. Su, "Blind image restoration based on $\ell_1 - \ell_2$ blur regularization," *Engineering Letters*, vol. 28, no. 1, pp. 148-154, 2020.

[18] I. Selesnick, "Sparse regularization via convex analysis," *IEEE Transactions on Signal Processing*, vol. 65, no. 17, pp. 4481-4494, 2017.

[19] I. Selesnick, A. Lanza, S. Morigi, et al, "Non-convex total variation regularization for convex denoising of signals," *Journal of Mathematical Imaging and Vision*, vol. 62, pp. 825-841, 2020.

[20] J. Zou, M. Shen, Y. Zhang, et al, "Total variation denoising with non-convex regularizers," *IEEE Access*, vol. 7, pp. 4422-4431, 2018.

[21] M. Shen, J. Li, T. Zhang and J. Zou, "Magnetic resonance imaging reconstructionvia non-convex total variation regularization," *International Journal of Imaging Systems and Technology*, pp. 1-13, Jul. 2020.

[22] Y. Liu, H. Du, Z. Wang, et al, "Convex MR brain image reconstruction via non-convex total variation minimization," *International Journal of Imaging Systems and Technology*, vol. 28, no. 4, pp. 246-253, 2018.

[23] S. Ramani and J. Fessler, "Parallel MR image reconstruction using augmented Lagrangian methods," *IEEE Transactions on Medical Imaging*, vol. 30, no. 3, pp. 694-706, 2011.

[24] J. Aelterman, H. Luong, B. Goossens, et al, "Augmented Lagrangian based reconstruction of non-uniformly sub-Nyquist sampled MRI data," *Signal processing*, vol. 91, no. 12, pp. 2731-2742, 2011.

[25] A. Chambolle and T. Pock, "A first-order primal-dual algorithm for convex problems with applications to imaging," *Journal of Mathematical Imaging and Vision*, vol. 40, no. 1, pp. 120-145, 2011.

[26] Y. Chen, W. Hager, F. Huang, et al, "Fast algorithms for image reconstruction with application to partially parallel MR imaging," *SIAM Journal on Imaging Sciences*, vol. 5, no. 1, pp. 90-118, 2012.

[27] X. Ye, Y. Chen and F. Huang, "Computational acceleration for MR image reconstruction in partially parallel imaging," *IEEE transactions on medical imaging*, vol. 30, no. 5, pp. 1055-1063, 2011.

[28] Y. Zhu and Y. Shi, "A fast method for reconstruction of total-variation MR images with a periodic boundary condition," *IEEE signal processing letters*, vol. 20, no. 4, pp. 291-294, 2013.

[29] J. Duan, Y. Liu and L. Zhang, "Bregman iteration based efficient algorithm for MR image reconstruction from undersampled K-space data," *IEEE Signal Processing Letters*, vol. 20, no. 8, pp. 831-834, 2013.

[30] A. Beck and M. Teboulle, " A fast iterative shrinkage-thresholding algorithm for linear inverse problems," *SIAM journal on imaging sciences*, vol. 2, no. 1, pp. 183-202, 2009.

[31] I. Daubechies, M. Defrise and C. De Mol, "An iterative thresholding algorithm for linear inverse problems with a sparsity constraint," *communications on pure & applied mathematics*, vol. 57, no. 11, pp. 1413-1457, 2003.

[32] S. Pejoski, V. Kafedziski and D.Gleich, "Compressed sensing MRI using discrete nonseparable shearlet transform and FISTA," *IEEE Signal Processing Letters*, vol. 22, no. 10, pp. 1566-1570, 2015.

[33] J. Cui, G. Peng, Q. Lu, et al, "Special regularized HSS iteration method for Tikhonov regularization,"*IAENG International Journal of Applied Mathematics*, vol. 50, no. 2, pp. 359-372, 2020.

[34] J. Yang, Y. Zhang and W. Yin, "A fast alternating direction method for TVL1-L2 signal reconstruction from partial fourier data," *IEEE Journal of Selected Topics in Signal Processing*, vol. 4, no. 2, pp. 288-297, 2010.

[35] Y. Yan, H. Li, Z. Xu, et al, "Deep ADMM-Net for compressive sensing MRI," *Advances in Neural Information Processing Systems*, Spain, pp. 10-18, 2016.

[36] B. Zhang and Z. Zhu, "Linearized proximal alternating direction method of multipliers for parallel magnetic resonance imaging," *IEEE/CAA Journal of Automatica Sinica*, vol. 4, no. 4, pp. 763-769, 2017.

[37] M. Le and J. Fessler, "Efficient convergent SENSE MRI reconstruction for nonperiodic boundary conditions via tridiagonal solvers," *IEEE Transactions on Computational Imaging*, vol. 3, no. 1, pp. 11-21, 2017.

[38] C. Lin and J. Fessler, "Efficient dynamic parallel MRI reconstruction for the low-rank plus sparse model," *IEEE Transactions on Computational Imaging*, vol. 5, no.1, pp. 17-26, 2018.

[39] J. Fessler, "Optimization methods for magnetic resonance image reconstruction: key models and optimization algorithms," *IEEE Signal Processing Magazine*, vol. 37, no. 1, pp. 33-40, 2020.

[40] B. He, F. Ma and X. Yuan, "Convergence study on the symmetric version of ADMM with larger step sizes," *SIAM journal on imaging sciences*, vol. 9, no. 3, pp. 1467-1501, 2016.

[41] Y. Liu, Z. Zhan, J. F. Cai, D. Guo and Z. Chen, "Projected iterative soft-thresholding algorithm for tight frames in compressed sensing magnetic resonance imaging," *IEEE Transactions on Medical Imaging*, vol. 35, no. 9, pp. 2130-2140, 2016.